

# ScalO-RAN: Energy-aware Network Intelligence Scaling in Open RAN

Stefano Maxenti<sup>\*†</sup>, Salvatore D'Oro<sup>\*</sup>, Leonardo Bonati<sup>\*</sup>, Michele Polese<sup>\*</sup>, Antonio Capone<sup>†</sup>, Tommaso Melodia<sup>\*</sup>

<sup>\*</sup>Institute for the Wireless Internet of Things, Northeastern University, Boston, MA, U.S.A.

<sup>†</sup>Politecnico di Milano, Milan, Italy

Email: {maxenti.s, s.doro, l.bonati, m.polese, melodia}@northeastern.edu, antonio.capone@polimi.it

**Abstract**—Network virtualization, software-defined infrastructure, and orchestration are pivotal elements in contemporary networks, yielding new vectors for optimization and novel capabilities. In line with these principles, O-RAN presents an avenue to bypass vendor lock-in, circumvent vertical configurations, enable network programmability, and facilitate integrated artificial intelligence (AI) support. Moreover, modern container orchestration frameworks (e.g., Kubernetes, Red Hat OpenShift) simplify the way cellular base stations, as well as the newly introduced RAN Intelligent Controllers (RICs), are deployed, managed, and orchestrated. While this enables cost reduction via infrastructure sharing, it also makes it more challenging to meet O-RAN control latency requirements, especially during peak resource utilization. For instance, the Near-real-time RIC is in charge of executing applications (xApps) that must take control decisions within one second, and we show that container platforms available today fail in guaranteeing such timing constraints. To address this problem, we propose ScalO-RAN, a control framework rooted in optimization and designed as an O-RAN rApp that allocates and scales AI-based O-RAN applications (xApps, rApps, dApps) to: (i) abide by application-specific latency requirements, and (ii) monetize the shared infrastructure while reducing energy consumption. We prototype ScalO-RAN on an OpenShift cluster with base stations, RIC, and a set of AI-based xApps deployed as micro-services. We evaluate ScalO-RAN both numerically and experimentally. Our results show that ScalO-RAN can optimally allocate and distribute O-RAN applications within available computing nodes to accommodate even stringent latency requirements. More importantly, we show that scaling O-RAN applications is primarily a time-constrained problem rather than a resource-constrained one, where scaling policies must account for stringent inference time of AI applications, and not only how many resources they consume.

**Index Terms**—O-RAN, Open RAN, Artificial Intelligence, Energy Efficiency, 5G, 6G.

## I. INTRODUCTION

The need for more flexible, energy-efficient, and cost-effective cellular networks—capable at the same time of delivering and guaranteeing high data rates and low latency—is driving the telco ecosystem toward Radio Access Network (RAN) cloudification. The shift leverages the principles of virtualization and softwarization, concepts deeply ingrained in

This work was partially supported by the National Telecommunications and Information Administration (NTIA)'s Public Wireless Supply Chain Innovation Fund (PWSCIF) under Award No. 25-60-IF002, and by OUSD(R&E) through Army Research Laboratory Cooperative Agreement Number W911NF-19-2-0221. The views and conclusions contained in this document are those of the authors and should not be interpreted as representing the official policies, either expressed or implied, of the Army Research Laboratory or the U.S. Government. The U.S. Government is authorized to reproduce and distribute reprints for Government purposes notwithstanding any copyright notation herein.

cloud-computing and internetworking fields via Software Defined Networking (SDN) and Network Functions Virtualization (NFV). These principles enable the design, development, and deployment of cellular networks with superior flexibility, which can be effectively monitored, controlled, optimized, upgraded, and reconfigured in real time via software.

This ongoing industry transformation has led to the Open RAN paradigm, and the creation of the O-RAN Alliance [1]. O-RAN leverages the principles described above to foster a cloud-based cellular architecture, with interoperable multi-vendor hardware and software components interconnected via open and standardized interfaces. It also embeds Artificial Intelligence (AI) and Machine Learning (ML) directly into the network to *forecast* loads, Key Performance Indicators (KPIs) and user mobility, *control* RAN functionalities and spectrum usage, and *classify* traffic profiles and identify anomalies, to name a few [1, 2]. To enable flexible 5G/6G networks, O-RAN introduces the concept of RAN Intelligent Controller (RIC), i.e., an abstraction enabling the execution of third-party network functions for AI-based inference and control. RICs are based on micro-services embedding intelligent workloads, called xApps and rApps. O-RAN defines specifically the Near-real-time (Near-RT) (hosting xApps) and the Non-real-time (Non-RT) RICs (hosting rApps) for inference loops up to 1 s and beyond 1 s, respectively. In addition, dApps have been proposed as micro-services for real-time inference ( $\leq 10$  ms) in the Central Units (CUs)/Distributed Units (DUs) [3].

The advantages of this cloud-based approach are: (i) it enables dynamic reconfiguration of the RAN by instantiating disaggregated functionalities, xApps and rApps on-the-fly to meet current demand and requirements [4–6]; and (ii) it reduces the total cost of ownership via cloud infrastructure sharing (i.e., sharing of data centers, servers and network equipment) [7].

However, RAN cloudification comes with possible downsides. First, it expands the compute surface, thus potentially increasing the power consumption of the RAN. Second, implementing intelligent control via micro-services in a cloud environment (called O-Cloud in O-RAN) may not provide tight performance guarantees required to close the control loops in the real, near-real, or non-real time scales. While timing constraints of virtualized RANs have been studied extensively in the literature with respect to the user plane [8–11], *how to achieve the same guarantees in the control plane is still an open challenge, especially regarding control loops and decisions made by the RICs*. Guaranteeing such constraints in the control

arXiv:2312.05096v2 [cs.NI] 15 Jan 2024

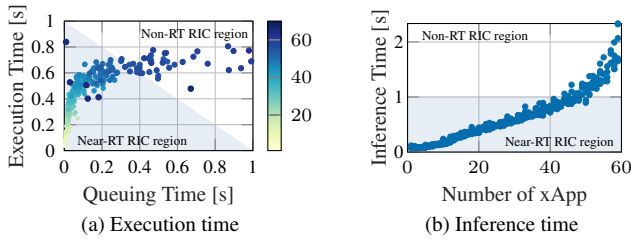


Fig. 1: Left: execution vs. queuing times for different xApp number. The number of xApps is indicated by the color map. Right: inference time vs. number of xApps. Shaded areas represent Near-RT RIC 1 s threshold.

plane is necessary to ensure that such decisions are timely and do not become obsolete by the time they are enforced.

Indeed, poorly-managed O-Cloud environments for rApps, xApps, and dApps can easily lead to control deadline violations, as shown in Fig. 1. Fig. 1a reports (i) the queuing time, i.e., the time needed by the Near-RT RIC to de-queue input data from the RAN and feed it to an xApp (x-axis); (ii) the execution time, i.e., the time needed by the xApp to process the input and generate an output (y-axis). Fig. 1b reports the inference time, i.e., the sum of queuing and execution time, with an increasing number of xApp (indicated by the colorbar in Fig. 1a) executed on the RIC. This example is based on measurements taken on an O-RAN-compliant Near-RT RIC deployed on a Red Hat OpenShift cluster, where we instantiate xApps with diverse AI workloads through the Continuous Integration (CI)/Continuous Deployment (CD) pipelines provided by NeutRAN [12]. The goal is to close the loop within the 1 s Near-RT RIC region (shaded areas in Fig. 1). In this case, the OpenShift fails to satisfy the control latency guarantees when the number of xApps exceeds 50, which is a conservative estimate for most real-world applications with hundreds of base stations [13].

In the cloud industry, compute resource scaling is an established strategy to cope with the need for extra processing power, and is a well-investigated topic in the literature [14–16], with a variety of approaches ranging from heuristic schedulers to predictive and ML-based models [17–24]. However, these solutions focus on ensuring that generic micro-services properly execute on the available compute resources, but *do not provide performance guarantees on latency-critical applications*. As an example, in a widely used framework like Kubernetes scaling is obtained either by regulating the amount of resources allocated to each service, or by increasing the number of active worker nodes in the compute cluster. However, this approach is based on resource utilization (e.g., CPU, RAM) and not on latency constraints (we will show that CPU/RAM-based scaling alone is unsuitable to ensure timely RAN control) [25]. Previous work has also addressed scaling with deadline constraints, but it considers long-term or stochastic latency metrics and leverage heuristic solutions rather than optimization [17, 26–29]. Moreover, uncontrolled and sub-optimal scaling might unnecessarily utilize excessive resources, thus increasing the energy consumption and costs (capital and operational), making the O-RAN proposition less attractive for network operators [30]. Therefore, *it is crucial to explore and understand this complex trade-off between latency and energy consumption*.

Our objective is to explore this trade-off and provide an optimization framework for scaling compute resources in the O-Cloud that is (i) aware of specific O-RAN application requirements; and (ii) satisfies inference constraints while minimizing energy consumption. We make the following contributions:

- We propose ScalO-RAN, a tunable auto-scaling framework for O-RAN systems, capable of managing AI-based xApps, rApps, and dApps on shared computing clusters with latency guarantees while considering important aspects such as profit and energy consumption (Secs. III and IV).
- We perform an extensive data collection campaign on the O-RAN Software Community (OSC) Near-RT RIC deployed on an OpenShift cluster to evaluate how resource sharing and scaling affect inference times of AI-based O-RAN applications (Sec. V). We leverage these measurements to derive a data-driven latency model that is used by ScalO-RAN to efficiently instantiate xApps, rApps, and dApps to satisfy application-specific latency requirements.
- We formulate the latency-constrained instantiation and scaling problem as a Quadratically Constrained Quadratic Problem (QCQP) that we prove NP-hard (Sec. VI). We solve the problem via branch-and-bound and evaluate ScalO-RAN’s effectiveness via simulations (Sec. VII). Results show that scaling O-RAN applications is a time-constrained problem where congestion is measured on how fast AI can produce outputs to guarantee continuous decision-making at diverse time scales, and not simply on how many resources are used.
- We prototype ScalO-RAN as an rApp and perform an extensive experimental campaign on an O-RAN-compliant testbed. Results show that ScalO-RAN can effectively perform instantiation and scaling tasks while guaranteeing desired application-specific latency requirements (Sec. VIII).

## II. RELATED WORK

Dynamic scaling of virtual machines or micro-services has been widely studied in the last decade [14, 15]. When considering scaling with latency guarantees, Singhvi et al. manage application latency with a deadline-aware scheduler in a serverless environment [17]. Mao et al. model virtual workload deadlines and costs, but for long-running applications rather than real, near-real, or non-real time control [26, 27]. Anagnostou et al. consider auto-scaling to meet deadlines for simulation workloads [28]. Das et al. [29] scale resources to meet query deadlines for a relational database, using a token bucket approach. Compared to prior work, in this paper we focus on tight control timelines, combine energy minimization or profit maximization, and scale resources solving a QCQP based on a detailed model of RAN control workloads.

Open RAN is extending the cloud domain to cellular network functions. Several virtual network function (VNF) scaling solutions have been proposed, but without considering latency guarantees for closed-loop control [31–33]. In the O-RAN context, Ali et al. analyze how to proactively scale resources for VNFs with workloads prediction [34]. D’Oro et al. orchestrate applications deployment, without however considering scaling or energy efficiency [35]. In the user plane, Garcia-Aviles et al.

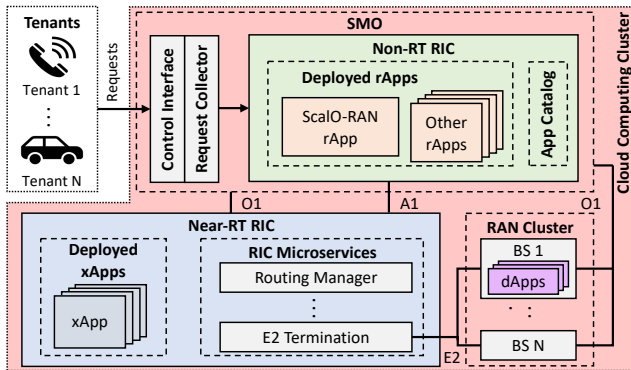


Fig. 2: ScalO-RAN within the O-RAN architecture.

design a framework to preserve synchronization among base stations and users, maximize network throughput, and save resources in the presence of computing capacity shortages [8]. Thaliath et al. [36] proactively scale resources to support network slices. However, these works are more concerned with optimally placing or executing services across the Open RAN infrastructure, rather than on guaranteeing control latency and minimizing energy consumption, as we do in this work.

Finally, energy efficiency is a priority for virtualized Open RAN. Prior literature work investigated energy consumption for the RAN—which consumes most of the energy in a cellular system [37]—as well as for VNFs (e.g., core network, RICs). Ayala-Romero et al. optimize virtualized RAN power consumption, evaluating waveform trade-offs in different signal-to-noise ratio regimes [38]. Pamuklu et al. propose a mixed linear programming problem for energy optimization, mindful of maximum tolerable delays for the data plane of the RAN [39]. Bonati et al. minimize RAN power consumption with dynamic power control orchestrated by a centralized controller [40]. Compared to these works, and to the best of our knowledge, ScalO-RAN is the first framework that optimally combines compute scaling, energy minimization, and timing constraints for RAN control in O-RAN, including an experimental inference characterization for different control workloads, and an experimental prototype.

### III. SCALO-RAN ARCHITECTURE AND PROTOTYPE

Fig. 2 illustrates ScalO-RAN and its integration with the O-RAN architecture. A set of tenants (e.g., network operators) interface with a *control interface* in the Service Management and Orchestration (SMO) to submit their request to deploy AI-based O-RAN applications. Requests are collected by a *request collector* hosted in the SMO, and forwarded to ScalO-RAN rApp every  $T$  seconds.  $T$  is a tunable parameter large enough to account for the time needed by ScalO-RAN *optimization engine* to compute a solution, and for the time needed to instantiate the requested rApps, xApps and dApps. After receiving these requests, ScalO-RAN computes an optimal instantiation and scaling policy to accommodate them, while making sure that demand and temporal constraints are satisfied (see Sec. VI for details on the optimization process). Then, rApps, xApps and dApps are instantiated from the *app catalog* to the selected servers—i.e., on the servers running the Non-RT RIC for rApps,

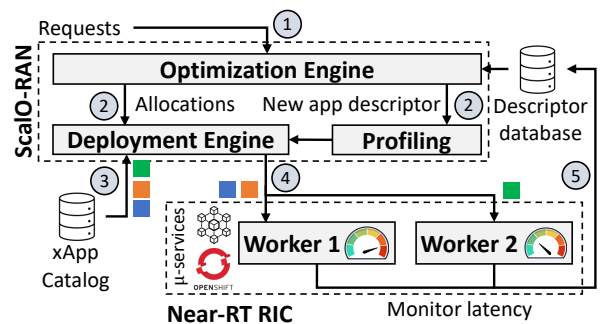


Fig. 3: ScalO-RAN OpenShift-based prototype.

Near-RT RIC for xApp, and CU/DU for dApps—according to the optimal solution found in the previous step.

**ScalO-RAN Prototype.** We prototype ScalO-RAN on a Red Hat OpenShift cluster with 8 Dell PowerEdge servers, i.e., 3 control nodes and 5 worker nodes—two of which are reserved for ScalO-RAN workloads—running various Open RAN components, e.g., OSC RICs, Open5GS core network, and cellular base stations based on srsRAN and OpenAirInterface. Fig. 3 depicts the main building blocks of our prototype, which implements ScalO-RAN procedures in steps 1-5 building on the CI/CD pipelines provided by NeutRAN [12]. The prototype enables latency profiling for xApps and embeds ScalO-RAN as an rApp to optimize workloads deployment. Although ScalO-RAN is general, our prototype focuses on xApp instantiation.

First, requests from the tenants to deploy xApps are received by the SMO, and forwarded to the ScalO-RAN optimization engine (Step 1). Each xApp is stored in a *App Catalog* and is assigned an *app descriptor* (Sec. IV) that specifies type, objective, input/output format of the embedded AI, among others. Upon receiving a request, ScalO-RAN controls whether the requested xApps are present in the catalog. New xApps (which lack of an app descriptor) are first profiled to benchmark their performance requirements (Step 2a), by deploying the xApp on an idle worker through ScalO-RAN deployment engine. xApp deployment on the Near-RT RIC is automated using the `dms_cli` tool and Helm charts [41]. In case of xApps with an app descriptor, the optimization engine computes the optimal xApp allocation policy (using MATLAB and Gurobi) to satisfy the received requests, and forwards the result to the deployment engine (Step 2b). The latter retrieves the xApps to instantiate from the xApp catalog (Step 3), and allocates them on the available worker nodes (e.g., worker 1 and worker 2 in the figure), based on the xApp latency constraints and on the expected run-time profile of the node (Step 4). Finally, the nodes of the cluster periodically report their run-time latency to ScalO-RAN control interface (Step 5).

### IV. SYSTEM MODEL

In this section, we introduce our system model and notation.

**Infrastructure.** We consider the Open RAN architecture proposed by the O-RAN Alliance [1]. The cloud infrastructure is represented by the O-Cloud, which hosts RAN functions (i.e., CUs, DUs, and Radio Units (RUs)), the Non-RT and Near-RT RICs, xApps, rApps, and the SMO framework. The O-Cloud

computing infrastructure has access to a set  $\mathcal{S}$  of  $S = |\mathcal{S}|$  servers. Although in principle servers in  $\mathcal{S}$  could also host RAN functions and RICs (see Fig. 2), data-driven O-RAN applications consume significant resources (e.g., CPU, RAM), and they might congest the server where they execute (see Fig. 1). To ensure reliability and availability of networking functionalities, we assume that rApps, xApps, and dApps execute on dedicated servers and let  $\mathcal{S}$  denote their set only. We also identify with  $\mathcal{S}^{\text{CU/DU}} \subseteq \mathcal{S}$  the servers co-located with a CU/DU that can host dApps. We design ScalO-RAN to be in charge of instantiating applications and scaling computing resources for a single cluster. In the case of  $C$  clusters,  $C$  instances of ScalO-RAN can be instantiated to serve each individual cluster.

**O-RAN applications.** The rApps, xApps, and dApps available to the tenants are stored in a catalog  $\mathcal{A}$  on the Non-RT RIC, with  $A = |\mathcal{A}|$  AI-based applications. Without loss of generality,  $\mathcal{A} = \mathcal{A}^{\text{rApp}} \cup \mathcal{A}^{\text{xApp}} \cup \mathcal{A}^{\text{dApp}}$ . Each application  $a \in \mathcal{A}$  is described via an *app descriptor* that specifies the delivered functionality (e.g., RAN slicing, traffic steering), the type of AI used (e.g., Deep Reinforcement Learning (DRL), Long Short Term Memory (LSTM), Convolutional Neural Network (CNN)), the type of application (e.g., xApp, rApp, dApp), the format and shape of input and output data (e.g., list of input KPIs and their shape, as well as type of action performed and its format), and its latency profile as detailed in Sec. V.

**Requests.** Tenants sharing the O-RAN infrastructure might have conflicting interest, different business goals, and serve users with different Service Level Agreements (SLAs). To satisfy these requirements and meet their goals, tenants submit requests to deploy a selection of rApps, xApps, and dApps from the catalog  $\mathcal{A}$ . Let  $\mathcal{R}$  be the set of requests submitted by all tenants. A request is modeled as a tuple  $r = (\mathbf{n}_r, \mathbf{L}_r, \boldsymbol{\delta}_r)$  where  $\mathbf{n}_r = (n_{r,a})_{(r,a) \in \mathcal{R} \times \mathcal{A}}$ ,  $\mathbf{L}_r = (L_{r,a})_{(r,a) \in \mathcal{R} \times \mathcal{A}}$ ,  $\boldsymbol{\delta}_r = (\delta_{r,a,s})_{(r,a,s) \in \mathcal{R} \times \mathcal{A} \times \mathcal{S}}$ , and  $\times$  indicates the Cartesian product.  $n_{r,a}$  represents the number of applications of type  $a \in \mathcal{A}$  that need to be instantiated to satisfy request  $r$ . Similarly,  $L_{r,a}$  represents the maximum inference time that the tenant tolerates executing applications of type  $a$  on any server. For example, a tenant could request  $n_{r,a'} = 4$  xApps to control RAN slicing policies of 4 DUs at a maximum tolerable inference time of  $L_{r,a'} = 100$  ms, as well as  $n_{r,a''} = 1$  rApp to control handover management with a desired inference time of  $L_{r,a''} = 10$  s. Note that controlling several RAN components with a single xApp/rApp is generally to be avoided, as it might result in congestion and large inference times. Hence, we assume  $n_{r,a} \geq 1$ .

Tenants might submit requests that do not require any maximum inference time guarantee (e.g.,  $L_{r,a} = +\infty$ ). However, by design the Near-RT RIC should take decisions within 1 s, while dApps should take decisions within 10 ms. For this reason, we also introduce a requirement  $L_a^{\text{APP}}$  that ensures that any application of type  $a$  produces an output within  $L_a^{\text{APP}}$ . For example, if application  $a \in \mathcal{A}^{\text{xApp}}$ ,  $L_a^{\text{APP}} = 1$  s, while  $L_a^{\text{APP}} = 10$  ms if  $a \in \mathcal{A}^{\text{dApp}}$ . Since O-RAN specifications do not provide any maximum inference time requirements for rApps, we set  $L_a^{\text{APP}} = +\infty$  for  $a \in \mathcal{A}^{\text{rApp}}$ .

We also introduce the parameter  $\delta_{r,a,s} \in \{0, 1\}$  to identify

the execution location of dApps. Specifically,  $\delta_{r,a,s} = 1$  indicates that a dApp  $a \in \mathcal{A}^{\text{dApp}}$  needs to be executed at server  $s$  co-located with a CU/DU. Since  $s$  unequivocally identifies each server, we can use  $s$  to identify the target CU/DU required by the tenant. We set  $\delta_{r,a,s} = 0$  for all  $a \in \mathcal{A} \setminus \mathcal{A}^{\text{dApp}}$  and servers.

#### A. Notation and variables

We introduce the server activation profile  $\mathbf{x} = (x_s)_{s \in \mathcal{S}}$ , where  $x_s \in \{0, 1\}$  indicates whether server  $s$  is actively hosting at least one AI-based O-RAN application ( $x_s = 1$ ) or not ( $x_s = 0$ ). To capture the allocation and instantiation of applications across the different servers, we introduce an allocation variable  $\mathbf{y} = (y_{r,a,s})_{(r,a,s) \in \mathcal{R} \times \mathcal{A} \times \mathcal{S}}$  that indicates how many instances of app  $a$  for request  $r$  have been instantiated on server  $s$ . For each request  $r$  and application  $a$ , the variables  $y_{r,a,s}$  are defined over the  $(A \cdot S - 1)$ -simplex  $\Delta_{r,a} = \{(y_{r,a,s})_{s \in \mathcal{S}}, y_{r,a,s} \in \mathbb{Z}_0^+ \mid \sum_{s \in \mathcal{S}} y_{r,a,s} = n_{r,a}\}$ , with  $\mathbb{Z}_0^+$  being the set of positive integer numbers including 0. It follows that  $x_s = 1$  if and only if  $\sum_{a \in \mathcal{A}} \sum_{r \in \mathcal{R}} y_{r,a,s} > 1$ . We introduce an auxiliary indicator variable  $w_{r,s} \in \{0, 1\}$  for all  $r \in \mathcal{R}$  and  $s \in \mathcal{S}$  such that  $w_{r,s} = 1$  if and only if  $\sum_{a \in \mathcal{A}} y_{r,a,s} > 0$ , i.e., server  $s$  is hosting at least one instance of any application required by request  $r$ .

We also introduce an indicator variable  $z_r \in \{0, 1\}$  that, for each  $r \in \mathcal{R}$ , represents whether the allocation variable  $\mathbf{y}$  satisfies the requirements of request  $r$ , both in terms of instances to be deployed, as well as latency ( $z_r = 1$ ), or not ( $z_r = 0$ ). We also define the indicator variable  $\pi_{a,s} \in \{0, 1\}$  to determine the number  $A_s$  of different applications that have at least one instance running on server  $s$ . For all  $a \in \mathcal{A}$  and  $s \in \mathcal{S}$ ,  $\pi_{a,s} = 1$  if server  $s$  has at least one instance of application  $a$ , i.e.,  $\sum_{r \in \mathcal{R}} y_{r,a,s} > 0$ , and  $\pi_{a,s} = 0$  otherwise.  $A_s$  is defined as:

$$A_s = \sum_a \pi_{a,s}. \quad (1)$$

Finally, we define the following variables,  $\mathbf{z} = (z_r)_{r \in \mathcal{R}}$ ,  $\mathbf{w} = (w_{r,s})_{(r,s) \in \mathcal{R} \times \mathcal{S}}$ , and  $\boldsymbol{\pi} = (\pi_{a,s})_{(a,s) \in \mathcal{A} \times \mathcal{S}}$ .

### V. INFERENCE TIME OF O-RAN APPLICATIONS

To properly satisfy inference constraints, we first derive a latency model to regulate scaling and instantiation procedures and ensure that all applications can close the control loop within the desired temporal window. This section reports the results of a data collection campaign, where we leverage the OpenShift ScalO-RAN prototype (Sec. III) to gather data on how congestion and resource sharing affect the inference time of different AI architectures and algorithms.

#### A. Profiling inference time

The inference time of AI-based O-RAN applications heavily depends on the complexity of the AI algorithms and architectures embedded in dApps, xApps, and rApps (e.g., width, depth, number of parameters and layers, need for convolutions). Moreover, as shown in Fig. 1, the more applications coexist on the same hardware and share its resources, the more the inference time increases due to constrained computational resources. Thus, to properly quantify how resource sharing of coexisting

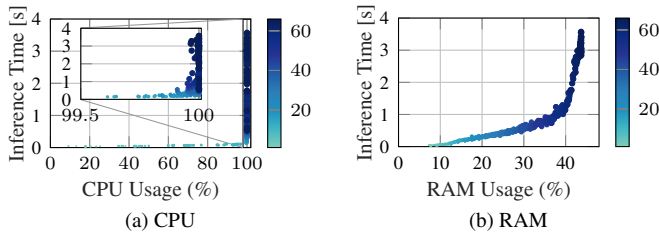


Fig. 4: Inference time vs. CPU and RAM usage for different number of xApps. The color map indicates the number of xApps.

applications affects their inference time, it is imperative to derive a model capable of capturing such dynamics.

AI for O-RAN systems can perform classification (e.g., anomaly detection), forecasting (e.g., KPI prediction), and control (e.g., resource allocation) [2]. Even if these tasks can be performed with multiple AI architectures (e.g., classification can use CNNs, Decision Trees), in our analysis we consider three well-established and diverse AI models for each of the above tasks. Specifically, for *classification*, we use a CNN with 231,875 parameters and a fully connected output layer; for *forecasting* we use a LSTM with 49,987 parameters, bidirectional memory cells, and a fully connected output layer; and for control we use a DRL agent with more than 50,000 parameters.

Our goal is to derive an inference time model to scale intelligent O-RAN applications. Thus, we only focus on evaluating their inference time, which is the same whether the AI has been trained or not, as the number of operations (e.g., multiplications, convolutions, additions) to perform is the same.

We consider a single worker node of the OpenShift cluster and we deploy one xApp instance at a time. To collect the data at scale, we developed an E2 traffic generator using the open-source O-RAN dataset from [42]. The generator emulates E2 traffic by constantly extracting at random KPIs from the dataset, with a format that matches the input expected by the xApp AI models (e.g., which KPI to extract and the shape of the input), as specified in the *app descriptor* of each xApp.

Whenever we add a new instance of xApp  $a$  on server  $s$ , we use the traffic generator to produce input data for the new instance and measure three types of latency: (i) *queuing time*  $t_{a,s}^{\text{queue}}$ , which measures how long it takes for the xApp to ingest the input once it has been received at the E2 termination of the Near-RT RIC; (ii) *execution time*  $t_{a,s}^{\text{exec}}$ , measuring the time to produce an output once an xApp receives an input; and (iii) *inference time*  $t_{a,s}^{\text{inf}} = t_{a,s}^{\text{queue}} + t_{a,s}^{\text{exec}}$ . We also keep track of CPU and RAM utilization of the server.

One could also consider both the time needed to forward the KPIs and the control action between the RAN and the RICs. However, since all servers are co-located in the same cluster, these parameters are constant. Moreover, data over high-speed optical fiber links has low and predictable latency (few hundreds of milliseconds, including switching), which is negligible if compared to the timescale of the Near-RT RIC (i.e., below 1 s) and Non-RT RIC (i.e., above 1 s). For these reasons, we do not include these terms in our model. Under these assumptions, we define the inference time when  $y$  instances of application

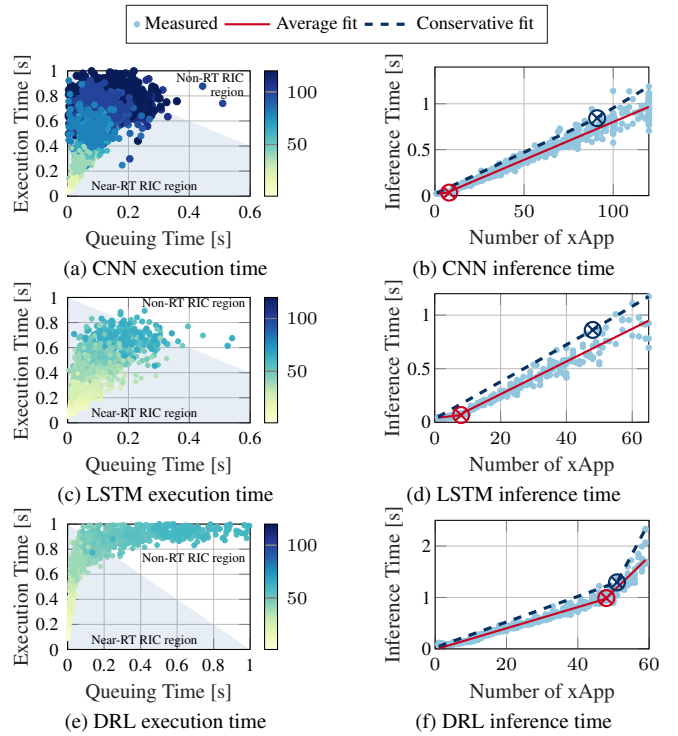


Fig. 5: Left: execution time vs. queuing time for different number of xApps. The color map indicates the number of xApps. Right: inference time vs. number of xApps.  $\otimes$  represents the break point of the piecewise linearization functions.

$a \in \mathcal{A}$  are executing on server  $s$  as follows:

$$t_{a,s}^{\text{inf}}(y) = t_{a,s}^{\text{exec}}(y) + t_{a,s}^{\text{queue}}(y). \quad (2)$$

### B. Deriving a latency model

In Fig. 4, we show how the inference time varies as a function of the CPU utilization and number of xApps (uniformly distributed between CNN, LSTM and DRL). We notice that 20 xApps already consume 100% of the CPU: this saturation prevents us from accurately modeling the execution time from the CPU utilization alone. RAM usage brings more insights, but predicting inference time from RAM occupation is hard as two models might use the same RAM but execute at different speeds. To overcome the above limitation, we instead focus on measuring both  $t_{a,s}^{\text{exec}}$  and  $t_{a,s}^{\text{queue}}$  and derive an inference time model from these parameters.

To better understand how execution and queuing time affect  $t_{a,s}^{\text{inf}}(y)$ , in Figs. 5a, 5c, and 5e we show  $t_{a,s}^{\text{exec}}(y)$  and  $t_{a,s}^{\text{queue}}(y)$  for the different xApp types when  $y$  instances of the same xApp execute on the server, while we show the respective  $t_{a,s}^{\text{inf}}(y)$  in Figs. 5b, 5d, and 5f. Instead, in Fig. 1 we present results obtained by instantiating  $y$  instances of the three xApps at the same time. The figures also show the regions identifying the Near-RT and Non-RT RICs operational domains. In general, we notice that the execution time  $t_{a,s}^{\text{exec}}(y)$  strongly affect inference time when  $y$  is small, while  $t_{a,s}^{\text{queue}}(y)$  becomes relevant when  $y$  grows due to congestion. These results suggest that inference time can be modeled using an increasing function with two distinct regions: a region where inference time grows at a

TABLE I: Piecewise Regression Parameters.

	Conservative fit					Average fit				
	$\lambda^I$	$b^I$	$\lambda^{II}$	$b^{II}$	$\tilde{y}$	$\lambda^I$	$b^I$	$\lambda^{II}$	$b^{II}$	$\tilde{y}$
CNN	9.057	18.94	11.73	-218.9	92	1.535	20.97	8.237	-22.3	9
LSTM	17.27	32.73	18.21	-10.68	49	3.498	38.99	15.26	-43.47	9
DRL	24.88	25.12	130	-5336	51	20.56	-10.54	67.45	-2250	48

moderate rate with the number of applications running on the server, and a congestion region with a steep increasing trend.

Although one can compute such functions in several ways (e.g., linear regression, neural networks), we aim at estimating latency with a model that is accurate, simple to integrate into an optimization problem, and reduces the underestimation risks to avoid deploying AI that would violate maximum latency requirements. For this reason, we model inference time via piecewise linear regression. This has several advantages: it is general, it can be used to accurately approximate non-linear functions, and can be used to remove non-linearities in optimization problems, thus resulting in lower complexity [43]. In general, one could compute the minimum amount of segments necessary for the approximation by using the piecewise linearization methods in [43]. However, our data analysis suggests that inference time behaves as an ‘‘elbow’’ function. We thus use 2-segment piecewise linear regression [44], which describes a function  $f(y)$  as  $f(y) = \lambda_1 \cdot y + b_1$  if  $y \leq y_0$ , and  $f(y) = \lambda_2 \cdot y + b_2$  if  $y > y_0$ , where  $y_0$  is the break point,  $\lambda_i$  is the slope and  $b_i$  is the intercept of the  $i$ -th segment.

Figs. 5b, 5d, and 5f also show that  $t_{a,s}^{\text{inf}}(y)$  can be approximated using the following 2-segment piecewise linear function

$$\tilde{t}_{a,s}^{\text{inf}}(y) = \begin{cases} \lambda_{a,s}^I \cdot y + b_{a,s}^I & \text{if } y \leq \tilde{y}_{a,s} \\ \lambda_{a,s}^{II} \cdot y + b_{a,s}^{II} & \text{otherwise,} \end{cases} \quad (3)$$

where  $\tilde{y}_{a,s}$  is the break point, and  $\lambda_{a,s}^i$  and  $b_{a,s}^i$  are the slope and intercept of the  $i$ -th segment, with  $i \in \{I, II\}$ . The values of  $\tilde{y}_{a,s}$ ,  $\lambda_{a,s}^I$ ,  $b_{a,s}^I$  and  $\lambda_{a,s}^{II}$  for the applications considered in our campaign are extracted via piecewise linear regression from the data collected on our prototype and are reported in Table I.

The figures illustrate the outcome of piecewise linearization of the inference time function for the ML-based control xApps for two cases: an *average fit* where we approximate the average behavior; and a *conservative fit* where we can account for upper bounds in the data via piecewise linear bounding [45]. We note that both linearization offers a good approximation that captures the elbow-shaped behavior of the distribution. The average fit might result in underestimations and violation of latency requirements, as it only captures the expected behavior. To mitigate this phenomenon, we can use the conservative fit which also accounts for the variance of measurements, especially when the number of deployed applications is high.

We now extend the application-specific inference model to a more general case where the same server hosts several instances of different applications. Note that while the measurement campaign profiled AI models packaged as xApps, the same latency model would hold when they are packaged as dApps or rApps. Let  $y_{r,a,s}$  be the number of instances of applications of

type  $a$  from any request  $r$  executing on server  $s$ . The inference time of all instances executing on server  $s$  can be expressed as

$$l_s(\mathbf{y}, \boldsymbol{\pi}) = \frac{1}{A_s} \sum_{a \in \mathcal{A}} \tilde{t}_{a,s}^{\text{inf}}(Y_s) \pi_{a,s}, \quad (4)$$

where  $Y_s = \sum_{r \in \mathcal{R}} \sum_{a \in \mathcal{A}} y_{r,a,s}$  is the total number of application instances hosted on  $s \in \mathcal{S}$ ,  $\tilde{t}_{a,s}^{\text{inf}}(\cdot)$  is defined in (3), and  $A_s$  from (1) is a function of  $\boldsymbol{\pi}$ . The expression in (4) models the expected value of the inference time when multiple instances of different applications are executed on the same server.

## VI. SCALO-RAN OPTIMIZATION ENGINE

In this section, we first introduce the instantiation and scaling problem for intelligent O-RAN applications. Then, we discuss how to design an objective function that can capture diverse needs such as reducing energy and maximizing profit.

### A. Formulating the problem

With the notation and variables defined in Sec. IV-A, we are ready to formulate the Instantiation and Scaling Problem (ISP):

$$\max_{\mathbf{x}, \mathbf{y}, \mathbf{z}, \mathbf{w}, \boldsymbol{\pi}} U(\mathbf{x}, \mathbf{y}, \mathbf{z}, \mathbf{w}, \boldsymbol{\pi}) \quad (\text{ISP})$$

$$\text{s.t.} : \sum_{s \in \mathcal{S}} y_{r,a,s} \geq n_{r,a} - M_1(1 - z_r), \quad \forall (r, a) \in \mathcal{R} \times \mathcal{A} \quad (5)$$

$$\sum_{s \in \mathcal{S}} y_{r,a,s} \leq n_{r,a} + M_1(1 - z_r), \quad \forall (r, a) \in \mathcal{R} \times \mathcal{A} \quad (6)$$

$$y_{r,a,s} \leq n_{r,a} \cdot x_s, \quad \forall (r, a, s) \in \mathcal{R} \times \mathcal{A} \times \mathcal{S} \quad (7)$$

$$l_s(\mathbf{y}, \boldsymbol{\pi}) w_{r,s} \leq L_{r,a}^{\text{MAX}}, \quad \forall (r, a, s) \in \mathcal{R} \times \mathcal{A} \times \mathcal{S} \quad (8)$$

$$\pi_{a,s} \leq x_s, \quad \forall (a, s) \in \mathcal{A} \times \mathcal{S} \quad (9)$$

$$\sum_{r \in \mathcal{R}} y_{r,a,s} \geq 1 - M_2(1 - \pi_{s,a}), \quad \forall (a, s) \in \mathcal{A} \times \mathcal{S} \quad (10)$$

$$\sum_{r \in \mathcal{R}} y_{r,a,s} \leq M_2 \cdot \pi_{s,a}, \quad \forall (a, s) \in \mathcal{A} \times \mathcal{S} \quad (11)$$

$$\sum_{a \in \mathcal{A}} y_{r,a,s} \geq 1 - M_3(1 - w_{r,s}), \quad \forall (r, s) \in \mathcal{R} \times \mathcal{S} \quad (12)$$

$$\sum_{a \in \mathcal{A}} y_{r,a,s} \leq M_3 \cdot w_{r,s}, \quad \forall (r, s) \in \mathcal{R} \times \mathcal{S} \quad (13)$$

$$w_{r,s} \geq -M_4(1 - x_s), \quad \forall (r, s) \in \mathcal{R} \times \mathcal{S} \quad (14)$$

$$w_{r,s} \leq M_4 \cdot x_s, \quad \forall (r, s) \in \mathcal{R} \times \mathcal{S} \quad (15)$$

$$w_{r,s} \leq z_r, \quad \forall (r, s) \in \mathcal{R} \times \mathcal{S} \quad (16)$$

$$y_{r,a,s} \leq \delta_{r,a,s}, \quad \forall (r, a, s) \in \mathcal{R} \times \mathcal{A} \times \mathcal{S} \quad (17)$$

where  $U(\cdot)$  is the objective function (which we will discuss in Sec. VI-B),  $L_{r,a}^{\text{MAX}} = \min\{L_{r,a}, L_a^{\text{APP}}\}$ ,  $l_s(\mathbf{y}, \boldsymbol{\pi})$  is defined in (4), and  $M_1 = M_2 = \sum_{a \in \mathcal{A}} n_{r,a} + 1$ ,  $M_3 = \max_{(r,a) \in \mathcal{R} \times \mathcal{A}} \{n_{r,a}\} + 1$ ,  $M_4 = 1$  are coefficients we use to formulate conditional constraints (e.g., applications can be instantiated on a server if and only if the server is active) using the big-M notation. Specifically, (5)-(6) ensure that a sufficient condition for a request  $r$  to be considered satisfied is that we must allocate all required applications and satisfy  $\mathbf{n}_r$ . (7) ensures that instances of application  $a$  requested by  $r$  can be instantiated only on active servers and the number of

instances cannot exceed the demand. (8) ensures that all latency requirements (from tenants or from O-RAN specifications) are satisfied. (9) ensures that application instances can run on active servers only, while (10)-(11) ensure that the indicator variable  $\pi_{a,s}$  is activated if and only if there is at least one instance of application of type  $a$  running on server  $s$ . Similarly, (12)-(15) ensure that  $w_{r,s} = 1$  if and only if there is at least one instance of any application requested by  $r$  running on an active server  $s$ . Finally, (16) ensures that  $w_{r,s} = 1$  only if the request can be satisfied completely (i.e., if  $z_r = 1$ ), and (17) guarantees that dApps are instantiated only at CUs and DUs selected by the tenants. From (3) and (1), (8) is non-linear but can be reformulated via the following big-M formulation

$$\sum_{a \in \mathcal{A}} \tilde{t}_{a,s}^{\text{inf}}(Y_s) \pi_{a,s} \leq L_{r,a}^{\text{MAX}} + M_5(1 - w_{r,s}), \quad (18)$$

where  $M_5$  is a large real-valued positive number, and  $\tilde{t}_{a,s}^{\text{inf}}(Y_s)$  is a piecewise function from (3) as follows

$$\begin{aligned} \tilde{t}_{a,s}^{\text{inf}}(Y_s) = & \nu_{a,s} (\lambda_{a,s}^I \cdot \sum_{r' \in \mathcal{R}} y_{r',a,s} + b_{a,s}^I) \\ & + (1 - \nu_{a,s}) \left( \lambda_{a,s}^I \cdot \tilde{y}_{a,s} + \lambda_{a,s}^{II} \sum_{r' \in \mathcal{R}} y_{r',a,s} \right) \end{aligned} \quad (19)$$

where  $\nu_{a,s} \in \{0, 1\}$  is an auxiliary variable that activates the first segment of the piecewise function if  $\sum_{r \in \mathcal{R}} y_{r,a,s} < \tilde{y}_{a,s}$ , or the second segment otherwise. Note that (19) is quadratic due to the products between  $\nu_{a,s}$  and  $y_{r',a,s}$ . However, these products can be linearized by adding auxiliary variables  $\tau_{r',a,s} \in \{0, 1\}$  such that  $\tau_{r',a,s} \leq \nu_{a,s}$  and  $\tau_{r',a,s} \leq y_{r',a,s}$ . By combining (19) and its linearization into (18), we obtain a quadratic constraint due to the product with  $\pi_{a,s}$ .

### B. Objective function design

Energy minimization is one of the major drivers of Open RAN, which can scale cloud compute on-the-fly to only activate the resources necessary for service delivery. To meet these expectations, we consider the total energy cost of activating servers and instantiating O-RAN applications:

$$E_s(x_s, \mathbf{y}_s) = x_s \cdot E_s^{\text{base}} + \sum_{a \in \mathcal{A}} \sum_{r \in \mathcal{R}} y_{r,a,s} e_{a,s}, \quad (20)$$

where  $\mathbf{y}_s = (y_{r,a,s})_{(r,a) \in \mathcal{R} \times \mathcal{A}}$ ,  $E_s^{\text{base}}$  represents the fixed amount of energy consumed by server  $s$  when turned on (i.e., with at least one application deployed), and  $e_{a,s}$  models the energy for an application of type  $a$ . (20) is based on experimental evidence showing that energy consumption scales linearly with the server load [46], represented here by the number of applications on the server (last term in (20)). Moreover,  $E_s(x_s, \mathbf{y}_s) = 0$  when  $x_s = 0$ , and (7) forces all  $y_{r,a,s} = 0$  to ensure applications selection prioritizes already active servers.

In general, infrastructure owners aim at maximizing their profit by minimizing the energy consumed to deliver the most valuable services. We formulate such energy-aware profit maximization problem with the following objective function:

$$U(\mathbf{x}, \mathbf{y}, \mathbf{z}) = \sum_{r \in \mathcal{R}} \rho_r z_r - \sigma \sum_{s \in \mathcal{S}} E_s(x_s, \mathbf{y}_s), \quad (21)$$

where  $\rho_r$  represents the monetary payment that the tenant is willing to pay to have their O-RAN applications deployed on the infrastructure,  $\sigma$  is the cost of energy expressed in monetary units per Joule, and  $E_s(\cdot)$  is defined in (20).

### C. Computational Complexity

**Theorem 1.** *Problem (ISP) is NP-hard.*

*Proof:* The proof is based on reducing the problem to the quadratically-constrained knapsack problem (QCKP), which is known to be NP-Hard [47]. Let us consider the case with  $S = 1$ ,  $\sum_{a \in \mathcal{A}} n_{r,a} = 1$  for all  $r \in \mathcal{R}$  (i.e., one application per request). Let us assume  $\delta_{r,a,s} = 1$  for all  $(r, a, s) \in \mathcal{R} \times \mathcal{A} \times \mathcal{S}$ , and  $L_{r,a}^{\text{MAX}} = L$  for all  $(r, a) \in \mathcal{R} \times \mathcal{A}$ , with  $L$  a small enough constant that prevents the use of the only server to accommodate all requests. Since each request is associated to one application only, let  $\lambda_r = \lambda_a(1)$ , where  $a$  is the only type of application requested. Recall that the latency function  $l_s(\cdot)$  in (8) is an increasing function in the number of requests hosted in each server, and each allocated request contributes with a factor  $\lambda_r$  to the total inference time. Problem (ISP) corresponds to an instance of the QCKP with one knapsack (the server) with capacity  $L$  (the inference time) and  $R$  objects (the requests) of value  $\rho_r$  and size  $\lambda_r$ , with a total value (monetary reward minus the cost) maximization goal. This problem is NP-hard [47] and we have built a polynomial-time reduction of the QCKP to an instance of Problem (ISP). Thus, Problem (ISP) is NP-hard by reduction unless  $P = NP$ . ■

Despite its NP-hardness, Problem (ISP) can be solved optimally via well-established optimization frameworks such as branch-and-bound [47]. In Sec. VII, we show that an optimal solution only requires a few seconds even for large instances of the problem with thousands of O-RAN applications, which is satisfactory and well within the non-real-time requirement of lifecycle management of O-RAN applications [1], and we also consider an approximation algorithm that offers lower complexity with slightly lower performance in terms of optimality.

## VII. PERFORMANCE EVALUATION

We numerically evaluate ScalO-RAN in MATLAB where we solve Problem (ISP) in Gurobi on a server with an Intel Core i9-9980HK CPU with 16 cores and 64 GB of RAM. For all simulations, we plot results averaged over 50 experiments.

We consider the 3 types of xApps in Table I and a conservative fit for (8). The idle energy is  $E_s^{\text{base}} = 360$  J (Dell PowerEdge R750) and  $e_{a,s} = \{8.77, 16, 22\}$  J for CNN, LSTM and DRL models by combining the inference/s time from Fig. 5 and the energy consumption per inference in [48]. The energy cost is  $\sigma = 0.165$  \$/kWh (current average in the U.S.).

We consider three possible *inference time profiles* such that  $L_{r,a} \in \{0.2, 1, 10\}$ s and consider the case where  $L_{r,a}^{\text{MAX}} = L_{r,a}$  for all  $(r, a) \in \mathcal{R} \times \mathcal{A}$ . We do not distinguish between dApps, xApps, and rApps, prioritizing the desired inference time required by each tenant. We refer to the above inference time profiles as Real-time (RT), Near-RT and Non-RT, respectively. For each request  $r$ , we set  $n_{r,a'} = n_{r,a''}$  for any  $(a', a'')$  and randomly select one inference time demand from the set defined

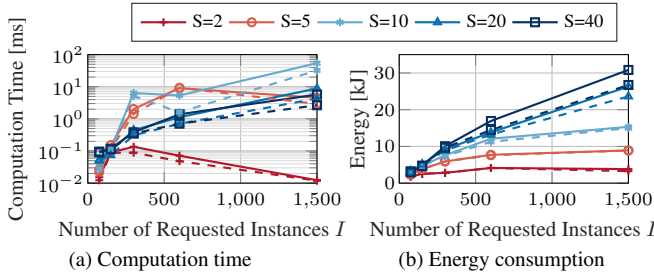


Fig. 6: Scalability and energy analysis for varying number of servers ( $S$ ) and number of instances ( $I$ ). Solid lines: optimal solution; dashed: early stopping.

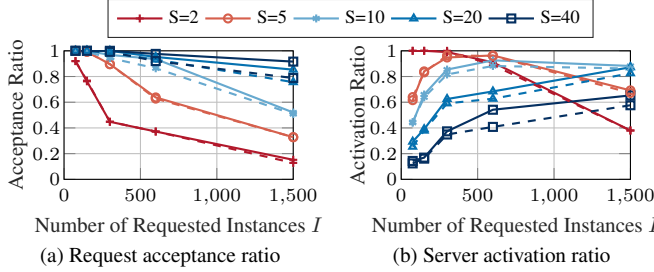


Fig. 7: Acceptance and activation ratios for varying number of servers ( $S$ ) and number of instances ( $I$ ). Solid lines: optimal solution; dashed: early stopping.

above with probability 10%, 60%, 30% for RT, Near-RT and Non-RT, respectively. In the following, we present results as a function of the *total number of instances* requested by all tenants which is defined as  $I = \sum_{r \in \mathcal{R}} \sum_{a \in \mathcal{A}} n_{r,a}$ . We consider homogeneous requests with same monetary value  $\rho_r = 2\$$  and same total number  $\sum_{a \in \mathcal{A}} n_{r,a}$  of application instances requested. The number of requests is  $R = 5$  and we vary  $\sum_{a \in \mathcal{A}} n_{r,a}$  to emulate very small or very large numbers of AI models for the control of a certain O-RAN deployment.

First, we analyze the *complexity* of solving Problem (ISP) optimally (solid lines in the figures). Fig. 6a shows the computation time as a function of  $I$  for different number of servers  $S$ . Intuitively, the complexity grows with the number of AI models ( $I$ ) to deploy up to a threshold  $I^*$ , where the trend reverses. As we show next (Fig. 8), this happens because for large  $I$  the optimization engine neglects requests with RT and Near-RT inference profiles, prioritizing Non-RT requests which can be satisfied in larger numbers. Indeed, the cost for accommodating RT and Near-RT requests is too high (they force a limit on the inference time for the entire server) as it prevents the admission of Non-RT requests. Thus, the algorithm discards their branches, converging faster to an optimal solution. We also compare against an approximation approach (dashed lines) where we perform early stopping on the branch-and-bound procedure when all reduced costs of the underlying dual problem are less than 0.01. As expected, early stopping produces sub-optimal solutions in less time, with a  $2.16 \times$  gain when  $S = 40$ .

Fig. 6b shows that the total *energy consumption* always increases with  $I$ , with a plateau when no more requests can be admitted. Early stopping computes solutions that consume less energy than the optimal. This is a consequence of its lower *acceptance ratio* (i.e., the ratio between the number of AI models actually instantiated and  $I$ , Fig. 7a) and lower *activation ratio* (i.e., the percentage of servers that host at least

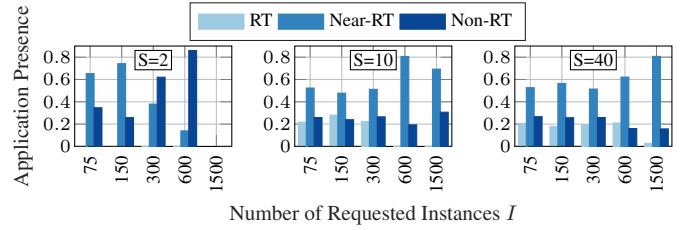


Fig. 8: Probability of a server to host a request with a certain inference time profile for varying number of servers ( $S$ ) and number of instances ( $I$ ).

one application, Fig. 7b). The optimal solution satisfies more than 90% of requests, with 65% servers activated when  $S = 40$ .

Fig. 7a shows that the acceptance ratio decreases with  $I$  and increases with larger number of available servers  $S$ . Differently, the activation ratio trend (Fig. 7b) is similar to that of the complexity (Fig. 6a). Indeed, when the number of servers  $S$  in the cluster is small, the activation ratio decreases with  $I$ , as it becomes impossible to allocate even a single RT or Near-RT without violating (8) with high probability.

Fig. 8 shows the *application presence* probability, i.e., the probability that requests with diverse inference time profiles are admitted by ScalO-RAN. When  $S = 2$ , RT requests are completely neglected, as they limit the number of admissible AI models.<sup>1</sup> Indeed, we see that with more servers it is possible to admit more RT and Near-RT requests. *These results clearly show that scaling AI solutions in O-RAN systems is not a resource-constrained problem, but a time-constrained one in that requirements on the inference time strongly affect how many dApps, xApps and rApps can coexist on the same server.*

Fig. 9 shows the probability that requests with diverse inference time profiles coexist on the same server. RT requests are less likely to share the same server with other profiles. For  $I \leq 300$ , both Near-RT and Non-RT requests can coexist with a probability higher than 0.5, which however drops to approximately 0.2 when  $I$  is large.

Finally, Fig. 10 compare ScalO-RAN against two other approaches, i.e., resource-based load balancing (native in OpenShift and frequently considered in the literature [14–16]) and no scaling, for  $S = 10$ . Load balancing distributes requests among servers based on congestion levels, while with no scaling all requests are instantiated on a single server. Load balancing and no scaling always admit all requests, while ScalO-RAN accepts  $\sim 98\%$  of requests when  $I = 300$  and 52% when  $I = 1500$ . Moreover, no scaling activates one server only, load balancing activates all servers, and ScalO-RAN activates on average 90% of servers. The lower ScalO-RAN acceptance and activation ratios are not a drawback, but a consequence of the energy-aware profit maximization objective coupled with the maximum inference time requirement. Together, these force ScalO-RAN to accept and distribute only those requests that guarantee timely inference time as requested by tenants.

Indeed, we see that no scaling is not suitable for O-RAN applications due to the extremely high inference time (Fig. 10).

<sup>1</sup>Constraint (8) forces a server to satisfy the latency requirement of the most demanding application being hosted in the server.

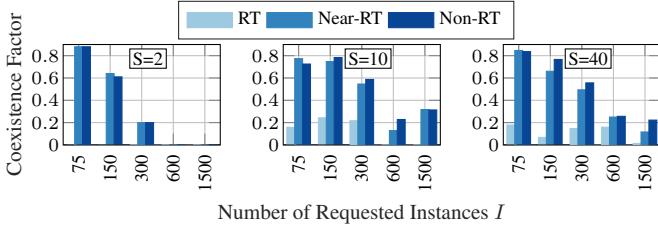


Fig. 9: Probability that requests with a certain inference time profile can coexist on the same server for varying number of servers ( $S$ ) and instances ( $I$ ).

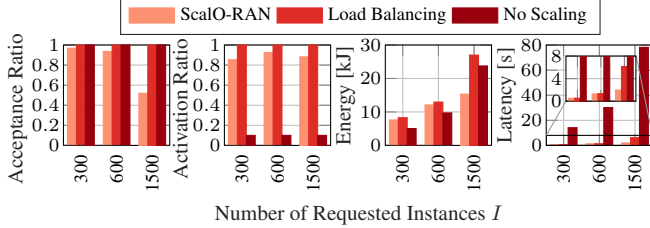


Fig. 10: ScalO-RAN vs. others for  $S = 10$  and varying number of instances ( $I$ ).

If compared to load balancing, ScalO-RAN provides a lower energy consumption and a lower inference time, which also satisfies timing requirements from tenants. Overall, ScalO-RAN performs better than widely used load balancing approaches by reducing energy while guaranteeing a timely inference.

### VIII. EXPERIMENTAL RESULTS

We use the prototype of Sec. III to experimentally evaluate ScalO-RAN and compare it against load balancing policies of OpenShift. We consider the same setup from Sec. VII with the three AI-based xApps in Fig. 5, the average fit in Table I and  $I = 123$  xApp instances to be deployed. Our prototype embeds two Dell PowerEdge R340 worker nodes (i.e.,  $WN_1$ ,  $WN_2$ , Fig. 3) used for xApp deployment, thus we consider  $R = 3$  tenants with one request each ( $r_1$ ,  $r_2$  and  $r_3$ ) to mimic a small O-RAN deployment. We consider Near-RT inference time profiles ([350, 1000] ms), and only  $r_1$  demands the maximum inference time of 350 ms. The monetary value is  $\rho_{r_1} = 30\rho_{r_2} = 30\rho_{r_3}$ .

Fig. 11 shows the CPU and RAM utilization over time for both ScalO-RAN and OpenShift for a single 4-minute experiment. Here, ScalO-RAN admits only requests  $r_1$  and  $r_2$  (demanding 350 ms and 1000 ms, respectively) instantiating 82 xApps, while OpenShift admits all requests and all 123 xApps. We notice that OpenShift allocates all xApps evenly across  $WN_1$  and  $WN_2$  due to load balancing. Instead, ScalO-RAN allocates instances in a more asymmetric way. Specifically, 85% of xApps on  $WN_1$  are from  $r_1$ , and the remaining 15% is from  $r_2$ . Instead, 100% of xApps on  $WN_2$  are from  $r_2$ . This allocation, especially the allocation on  $WN_1$ , ensures that all xApps satisfy the 350 ms inference constraint on  $WN_1$  as required by  $r_1$ . Instead, CPU usage is almost 100% except for the initial deployment phase. The allocation phase is voluntarily slow, as we allocate one xApp at a time to collect reliable data.

Fig. 12 reports the inference time over time for ScalO-RAN and OpenShift. We clearly see that OpenShift cannot satisfy even the 1000 ms requirement, as it allocates all xApps without considering their timing requirements. This results in inference

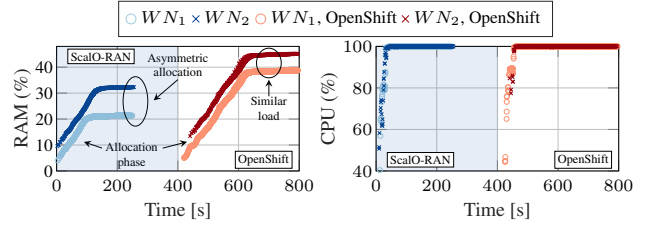


Fig. 11: RAM and CPU utilization over time with ScalO-RAN and OpenShift.

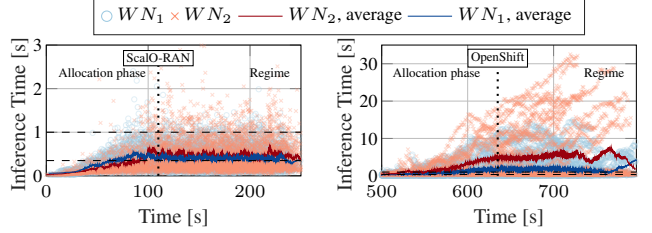


Fig. 12: Evolution of the inference time with ScalO-RAN and OpenShift.

time violations that affect the proper functioning of the RAN. Instead, ScalO-RAN not only admits requests whose demands can be accommodated, but distributes xApps to ensure that  $WN_1$  (which hosts all xApps of  $r_1$  and 15% of xApps of  $r_2$ ) delivers the 350 ms requirements on average, while  $WN_2$  can guarantee the 1000 ms requirement from  $r_2$ . Finally, in Fig. 13

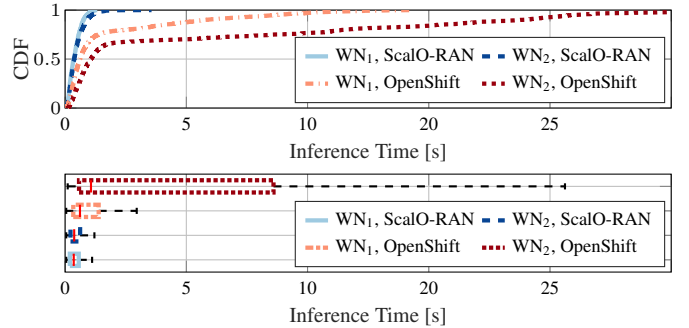


Fig. 13: CDF and boxplot of inference time with ScalO-RAN and OpenShift.

we show the Cumulative Distribution Function (CDF) for the different worker nodes and approaches, as well as the boxplots showing median values. We see that OpenShift cannot guarantee any inference time demand, while ScalO-RAN ensures that the expected inference time follows tenant requirements.

### IX. CONCLUSIONS

In this work, we presented ScalO-RAN, an O-RAN energy-aware scaling system to enforce inference time constraints on intelligent applications. We provided a latency model based on a measurement campaign on an OpenShift cluster, a mathematical optimization model, and an O-RAN-compliant prototype. We compared ScalO-RAN with OpenShift's scaling mechanism, showing that ScalO-RAN is able to deploy O-RAN applications complying with the operators' latency constraints. Results demonstrate that scaling AI solutions in O-RAN is not resource-constrained only, but also time-constrained as requirements on the inference time strongly affect how many dApps, xApps and rApps can coexist on the same server.

## REFERENCES

- [1] M. Polese, L. Bonati, S. D'Oro, S. Basagni, and T. Melodia, "Understanding O-RAN: Architecture, Interfaces, Algorithms, Security, and Research Challenges," *IEEE Communications Surveys & Tutorials*, 2023.
- [2] B. Brik, K. Boutiba, and A. Ksentini, "Deep Learning for B5G Open Radio Access Network: Evolution, Survey, Case Studies, and Challenges," *IEEE Open Journal of the Communications Society*, vol. 3, 2022.
- [3] S. D'Oro, M. Polese, L. Bonati, H. Cheng, and T. Melodia, "dApps: Distributed Applications for Real-Time Inference and Control in O-RAN," *IEEE Communications Magazine*, vol. 60, no. 11, 2022.
- [4] R. Schmidt and N. Nikaiein, "RAN Engine: Service-Oriented RAN Through Containerized Micro-Services," *IEEE Transactions on Network and Service Management*, vol. 18, no. 1, pp. 469–481, March 2021.
- [5] S. Niknam, A. Roy, H. S. Dhillon, S. Singh, R. Banerji, J. H. Reed, N. Saxena, and S. Yoon, "Intelligent O-RAN for Beyond 5G and 6G Wireless Networks," in *IEEE Globecom Workshops*, December 2022.
- [6] L. Bonati, S. D'Oro, M. Polese, S. Basagni, and T. Melodia, "Intelligence and Learning in O-RAN for Data-driven NextG Cellular Networks," *IEEE Communications Magazine*, vol. 59, no. 10, pp. 21–27, October 2021.
- [7] B. Ojaghi, F. Adelantado, and C. Verikoukis, "On the Benefits of vDU Standardization in Software-defined NG-RAN: Enabling Technologies, Challenges, and Opportunities," *IEEE Communications Magazine*, vol. 61, no. 4, pp. 92–98, April 2023.
- [8] G. Garcia-Aviles, A. Garcia-Saavedra, M. Gramaglia, X. Costa-Perez, P. Serrano, and A. Banchs, "Nuberu: Reliable RAN Virtualization in Shared Platforms," in *Proc. of ACM MobiCom*, October 2021.
- [9] A. Garcia-Saavedra, X. Costa-Perez, D. J. Leith, and G. Iosifidis, "FluidRAN: Optimized vRAN/MEC Orchestration," in *Proc. of IEEE INFOCOM*, April 2018.
- [10] I. Parvez, A. Rahmati, I. Guvenc, A. I. Sarwat, and H. Dai, "A Survey on Low Latency Towards 5G: RAN, Core Network and Caching Solutions," *IEEE Communications Surveys & Tutorials*, vol. 20, no. 4, 2018.
- [11] F. Giannone, K. Kondepu, H. Gupta, F. Civerchia, P. Castoldi, A. Antony Franklin, and L. Valcarenghi, "Impact of Virtualization Technologies on Virtualized RAN Midhaul Latency Budget: A Quantitative Experimental Evaluation," *IEEE Communications Letters*, vol. 23, no. 4, pp. 604–607, April 2019.
- [12] L. Bonati, M. Polese, S. D'Oro, S. Basagni, and T. Melodia, "NeutRAN: An Open RAN Neutral Host Architecture for Zero-Touch RAN and Spectrum Sharing," *IEEE Transactions on Mobile Computing*, 2023.
- [13] M. Polese, R. Jana, V. Kounev, K. Zhang, S. Deb, and M. Zorzi, "Machine Learning at the Edge: A Data-Driven Architecture With Applications to 5G Cellular Networks," *IEEE Transactions on Mobile Computing*, vol. 20, no. 12, pp. 3367–3382, December 2021.
- [14] L. M. Vaquero, L. Rodero-Merino, and R. Buyya, "Dynamically Scaling Applications in the Cloud," *SIGCOMM Computer Communication Review*, vol. 41, no. 1, p. 45–52, January 2011.
- [15] A. Bauer, V. Lesch, L. Versluis, A. Ilyushkin, N. Herbst, and S. Kounev, "Chamulteon: Coordinated Auto-Scaling of Micro-Services," in *Proc. of IEEE ICDCS*, July 2019.
- [16] A. Gulati, G. Shanmuganathan, A. Holler, and I. Ahmad, "Cloud Scale Resource Management: Challenges and Techniques," in *Proc. of USENIX HotCloud*, 2011.
- [17] A. Singhvi, A. Balasubramanian, K. Houck, M. D. Shaikh, S. Venkataraman, and A. Akella, "Atoll: A Scalable Low-Latency Serverless Platform," in *Proc. of ACM Symposium on Cloud Computing*, 2021.
- [18] T. Hu and Y. Wang, "A Kubernetes Autoscaler Based on Pod Replicas Prediction," in *Asia-Pacific Conference on Communications Technology and Computer Science (ACCTCS)*, Jan 2021, pp. 238–241.
- [19] F. Rossi, M. Nardelli, and V. Cardellini, "Horizontal and Vertical Scaling of Container-Based Applications Using Reinforcement Learning," in *Proc. of IEEE CLOUD*, July 2019.
- [20] E. Casalicchio and V. Perciballi, "Auto-Scaling of Containers: The Impact of Relative and Absolute Metrics," in *Proc. of IEEE FAS\*W*, 2017.
- [21] L. Abeni and D. Faggioli, "Using Xen and KVM as Real-time Hypervisors," *Journal of Systems Architecture*, vol. 106, p. 101709, 2020.
- [22] A. Di Stefano, A. Di Stefano, and G. Morana, "Ananke: A Framework for Cloud-Native Applications Smart Orchestration," in *Proc. of IEEE WETICE*, 2020.
- [23] I. Prachitmutita, W. Aittinonmongkol, N. Pojjanasuksakul, M. Supattatham, and P. Padungweang, "Auto-scaling Microservices on IaaS Under SLA with Cost-effective Framework," in *Proc. of IEEE ICACI*, 2018.
- [24] R. Han, L. Guo, M. M. Ghanem, and Y. Guo, "Lightweight Resource Scaling for Cloud Applications," in *Proc. of IEEE/ACM CCGrid*, 2012.
- [25] Kubernetes, "Horizontal Pod Autoscaling," 2023. [Online]. Available: <https://tinyurl.com/5n8jykm3>
- [26] M. Mao, J. Li, and M. Humphrey, "Cloud Auto-scaling with Deadline and Budget Constraints," in *Proc. of IEEE/ACM International Conference on Grid Computing*, 2010.
- [27] M. Mao and M. Humphrey, "Auto-Scaling to Minimize Cost and Meet Application Deadlines in Cloud Workflows," in *Proc. of International Conference for High Performance Computing, Networking, Storage and Analysis*, 2011.
- [28] A. Anagnostou, S. J. E. Taylor, N. Tijjani Abubakar, T. Kiss, J. DesLauriers, G. Gesmier, G. Terstyanszky, P. Kacsuk, and J. Kovacs, "Towards a Deadline-Based Simulation Experimentation Framework Using Micro-Services Auto-Scaling Approach," in *Proc. of IEEE WSC*, 2019.
- [29] S. Das, F. Li, V. R. Narasayya, and A. C. König, "Automated demand-driven resource scaling in relational database-as-a-service," in *Proc. ACM International Conference on Management of Data*, 2016.
- [30] M. Hoffmann and M. Dryjański, "The O-RAN Whitepaper 2023: Energy Efficiency in O-RAN," Rimedo Labs White Paper. [Online]. Available: <https://tinyurl.com/ys7mmk69>
- [31] X. Fei, F. Liu, H. Xu, and H. Jin, "Adaptive VNF Scaling and Flow Routing with Proactive Demand Prediction," in *Proc. of IEEE INFOCOM*, April 2018.
- [32] Y. Bi, C. Colman-Meixner, R. Wang, F. Meng, R. Nejabati, and D. Simeonidou, "Resource Allocation for Ultra-Low Latency Virtual Network Services in Hierarchical 5G Network," in *Proc. of IEEE ICC*, 2019.
- [33] D. Harutyunyan, R. Behraves, and N. Slamnuk-Kriještorac, "Cost-efficient Placement and Scaling of 5G Core Network and MEC-enabled Application VNFs," in *Proc. of IFIP/IEEE International Symposium on Integrated Network Management (IM)*, 2021.
- [34] K. Ali and M. Jammal, "Proactive VNF Scaling and Placement in 5G O-RAN using ML," *IEEE Transactions on Network and Service Management*, 2023.
- [35] S. D'Oro, L. Bonati, M. Polese, and T. Melodia, "OrchestRAN: Network Automation through Orchestrated Intelligence in the Open RAN," in *Proc. of IEEE INFOCOM*, May 2022.
- [36] J. Thaliath, S. Niknam, S. Singh, R. Banerji, N. Saxena, H. S. Dhillon, J. H. Reed, A. K. Bashir, A. Bhat, and A. Roy, "Predictive Closed-Loop Service Automation in O-RAN Based Network Slicing," *IEEE Communications Standards Magazine*, vol. 6, no. 3, pp. 8–14, Sep. 2022.
- [37] A. Capone, S. D'Elia, I. Filippini, A. E. C. Redondi, and M. Zangani, "Modeling energy consumption of mobile radio networks: An operator perspective," *IEEE Wireless Communications*, vol. 24, no. 4, 2017.
- [38] J. A. Ayala-Romero, I. Khalid, A. Garcia-Saavedra, X. Costa-Perez, and G. Iosifidis, "Experimental Evaluation of Power Consumption in Virtualized Base Stations," in *Proc. of IEEE ICC*, 2021.
- [39] T. Pamuklu, S. Mollahasani, and M. Erol-Kantarci, "Energy-Efficient and Delay-Guaranteed Joint Resource Allocation and DU Selection in O-RAN," in *Proc. of IEEE 5GWF*, October 2021.
- [40] L. Bonati, S. D'Oro, L. Bertizzolo, E. Demirors, Z. Guan, S. Basagni, and T. Melodia, "CellOS: Zero-touch Software-defined Open Cellular Networks," *Computer Networks*, vol. 180, pp. 1–13, October 2020.
- [41] "Installation of the OSC Near-real-time RIC," <https://shorturl.at/sv135>.
- [42] M. Polese, L. Bonati, S. D'Oro, S. Basagni, and T. Melodia, "CoLO-RAN: Developing Machine Learning-based xApps for Open RAN Closed-loop Control on Programmable Experimental Platforms," *IEEE Transactions on Mobile Computing*, pp. 1–14, July 2022.
- [43] J. G. Dunham, "Optimum Uniform Piecewise Linear Approximation of Planar Curves," *IEEE Transactions on Pattern Analysis and Machine Intelligence*, no. 1, pp. 67–75, 1986.
- [44] E. Vieth, "Fitting piecewise linear regression functions to biological responses," *Journal of applied physiology*, vol. 67, no. 1, 1989.
- [45] S. U. Ngueveu, "Piecewise Linear Bounding of Univariate Nonlinear Functions and Resulting Mixed Integer Linear Programming-based Solution Methods," *European Journal of Operational Research*, vol. 275, no. 3, pp. 1058–1071, 2019.
- [46] X. Fan, W.-D. Weber, and L. A. Barroso, "Power Provisioning for a Warehouse-sized Computer," *ACM SIGARCH Computer Architecture News*, vol. 35, no. 2, pp. 13–23, 2007.
- [47] M. Klimm, M. E. Pfetsch, R. Raber, and M. Skutella, "Packing under convex quadratic constraints," *Mathematical Programming*, vol. 192, no. 1–2, pp. 361–386, 2022.
- [48] C. Baskin, N. Liss, E. Zheltonozhskii, A. M. Bronstein, and A. Mendelson, "Streaming Architecture for Large-scale Quantized Neural Networks on an FPGA-based Dataflow Platform," in *Proc. of IEEE IPDPSW*, 2018.